INSTITUTE OF PHYSICS PUBLISHING JOURNAL OF PHYSICS: CONDENSED MATTER

J. Phys.: Condens. Matter **17** (2005) 1085–1097 doi:10.1088/0953-8984/17/7/003

Polar optical phonons in wurtzite spheroidal quantum dots: theory and application to ZnO and ZnO/MgZnO nanostructures

Vladimir A Fonoberov and Alexander A Balandin

Nano-Device Laboratory, Department of Electrical Engineering, University of California Riverside, Riverside, CA 92521, USA

E-mail: vladimir@ee.ucr.edu and alexb@ee.ucr.edu

Received 10 December 2004, in final form 12 January 2005
Published 4 February 2005
Online at stacks.iop.org/JPhysCM/17/1085

Abstract

Polar optical-phonon modes are derived analytically for spheroidal quantum dots with wurtzite crystal structure. The developed theory is applied to freestanding spheroidal ZnO quantum dots and to spheroidal ZnO quantum dots embedded into a MgZnO crystal. The wurtzite (anisotropic) quantum dots are shown to have strongly different polar optical-phonon modes in comparison with zincblende (isotropic) quantum dots. The obtained results allow one to explain and accurately predict phonon peaks in the Raman spectra of wurtzite nanocrystals, nanorods (prolate spheroids), and epitaxial quantum dots (oblate spheroids).

(Some figures in this article are in colour only in the electronic version)

1. Introduction

It is well known that in quantum dots with zincblende crystal structure there exist confined phonon modes with the frequencies equal to those of bulk transverse optical (TO) and longitudinal optical (LO) phonons and interface phonon modes with the frequencies intermediate between those of TO and LO modes [1]. Interface and confined optical phonon modes have been found for a variety of zincblende quantum dots such as spherical [1], spheroidal [2, 3], multilayer spherical [4], and even multilayer tetrahedral [5] quantum dots. The calculated frequencies of optical phonon modes have been observed in the Raman, absorption, and photoluminescence spectra of zincblende quantum dots [5, 6]. Lately, quantum dots with wurtzite crystal structure, such as ZnO and GaN nanostructures, have attracted attention as very promising candidates for optoelectronic, electronic, and biological applications. At the same time, only a few reports have addressed the problem of polar optical phonons in wurtzite nanostructures [7, 8]. The solution obtained in [7] is approximate, i.e. uses

Table 1. Optical dielectric constants and frequencies of polar optical phonons for two wurtzite crystals. The values for ZnO are from [11] and the values for $Mg_{0.2}Zn_{0.8}O$ are from [12].

Wurtzite crystal	$\varepsilon_z(\infty)$ $= \varepsilon_\perp(\infty)$	$\omega_{z,\mathrm{LO}}$ (cm^{-1})	$\omega_{z,\mathrm{TO}}$ (cm^{-1})	$\omega_{\perp 1,\mathrm{LO}}$ (cm^{-1})	$\omega_{\perp 1,\mathrm{TO}}$ (cm^{-1})	$\omega_{\perp 2,\mathrm{LO}}$ (cm^{-1})	$\omega_{\perp 2,\mathrm{TO}}$ (cm^{-1})
ZnO	3.70	579	380	591	413		
$Mg_{0.2}Zn_{0.8}O$	3.41	586	384	505	417	635	525

a priori selected exponential dependence for the phonon potential, and provides an estimate only for interface optical phonon modes.

The frequencies of optical phonons in small covalent nanocrystals depend on the nanocrystal size, because the nanocrystal boundary causes an uncertainty in the phonon wavevector, which results in the redshift and broadening of the phonon peak. While the above size dependence is important for very small covalent nanocrystals, it is negligible in the ionic ZnO quantum dots with sizes larger than 4 nm. The latter is due to the fact that the polar optical phonons in ZnO are almost non-dispersive in the region of small wavevectors. Since most of the reported experimental data are for ZnO quantum dots with sizes larger than 4 nm, in the following we assume that the polar optical phonons are non-dispersive in the relevant range of the wavevectors. Due to the uniaxial anisotropy of wurtzite quantum dots, the confined and interface optical phonon modes in such quantum dots should be substantially different from those in zincblende (isotropic) quantum dots [8]. The main difference comes from the anisotropy of the dielectric function of wurtzite crystals. In order to describe the dielectric function, we employ the Loudon model, which is widely accepted for the wurtzite nanostructures [9, 10]. For example, the components of the dielectric tensor of wurtzite ZnO are [11]

$$\varepsilon_\perp(\omega) = \varepsilon_\perp(\infty)\frac{\omega^2 - (\omega_{\perp,\mathrm{LO}})^2}{\omega^2 - (\omega_{\perp,\mathrm{TO}})^2}; \qquad \varepsilon_z(\omega) = \varepsilon_z(\infty)\frac{\omega^2 - (\omega_{z,\mathrm{LO}})^2}{\omega^2 - (\omega_{z,\mathrm{TO}})^2}, \tag{1}$$

where the optical dielectric constants $\varepsilon_\perp(\infty)$ and $\varepsilon_z(\infty)$, LO phonon frequencies $\omega_{\perp,\mathrm{LO}}$ and $\omega_{z,\mathrm{LO}}$, and TO phonon frequencies $\omega_{\perp,\mathrm{TO}}$ and $\omega_{z,\mathrm{TO}}$ of bulk wurtzite ZnO are listed in table 1. The components of the dielectric tensor of some ternary wurtzite crystals such as $Mg_xZn_{1-x}O$ ($x < 0.33$) have more complex frequency dependence [12]:

$$\varepsilon_\perp(\omega) = \varepsilon_\perp(\infty)\frac{\omega^2 - (\omega_{\perp 1,\mathrm{LO}})^2}{\omega^2 - (\omega_{\perp 1,\mathrm{TO}})^2}\frac{\omega^2 - (\omega_{\perp 2,\mathrm{LO}})^2}{\omega^2 - (\omega_{\perp 2,\mathrm{TO}})^2}; \qquad \varepsilon_z(\omega) = \varepsilon_z(\infty)\frac{\omega^2 - (\omega_{z,\mathrm{LO}})^2}{\omega^2 - (\omega_{z,\mathrm{TO}})^2}. \tag{2}$$

The corresponding material parameters from equation (2) for bulk wurtzite $Mg_{0.2}Zn_{0.8}O$ are also listed in table 1. Zone centre optical phonon frequencies of wurtzite ZnO and $Mg_{0.2}Zn_{0.8}O$ are shown in figure 1. Since there are only two zone centre optical phonon frequencies (one LO and one TO) in zincblende crystals, the phonon band structure of wurtzite crystals is more complex than that of zincblende crystals. It will be shown in the following that the latter fact leads to polar optical phonon modes in wurtzite quantum dots that are strongly different from those in zincblende quantum dots.

The rest of the paper is organized as follows. In section 2 we present the analytical derivation of the polar optical phonon modes in spheroidal quantum dots with wurtzite crystal structure. In sections 3 and 4, the developed theory is applied to a freestanding spheroidal ZnO quantum dot and to a spheroidal ZnO quantum dot embedded into an $Mg_{0.2}Zn_{0.8}O$ crystal, correspondingly. Conclusions are given in section 5.

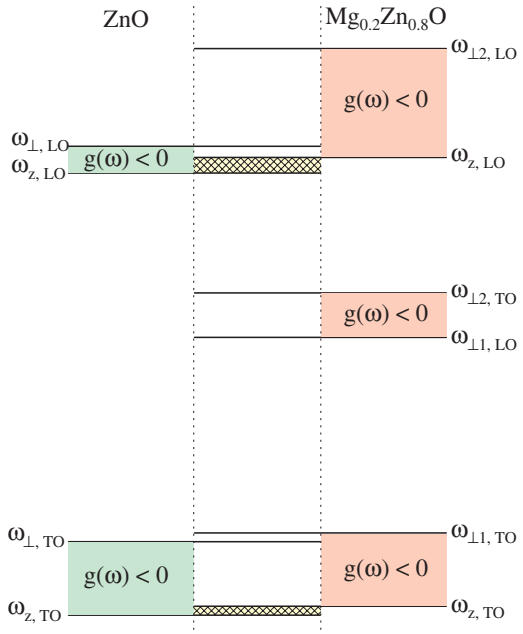

Figure 1. Zone centre optical phonon frequencies of ZnO and $Mg_{0.2}Zn_{0.8}O$. Shaded regions correspond to the condition $g(\omega) < 0$ (see equation (15)). Cross-hatched regions correspond to the condition $g(\omega) < 0$ for ZnO and $g(\omega) > 0$ for $Mg_{0.2}Zn_{0.8}O$.

2. Theory

Let us consider a spheroidal quantum dot with wurtzite crystal structure and with semi-axes a and c. The coordinate system $(x,\ y,\ z')$ is chosen in such a way that the semi-axis c is directed along the symmetry axis z' of the quantum dot. The equation of the quantum dot surface is

$$\frac{x^2+y^2}{a^2}+\frac{z'^2}{c^2}=1. \tag{3}$$

After we introduce a new coordinate z such as

$$z'=\frac{c}{a}z \tag{4}$$

and transform the new Cartesian coordinates $(x,\ y,\ z)$ into spherical coordinates (r,θ,ϕ), the equation (3) of the quantum dot surface becomes $r=a$. In the following derivation we assume that the quantum dot (medium $k=1$) is embedded in a wurtzite crystal (medium $k=2$). A freestanding quantum dot can be easily considered as a special case.

Within the framework of the dielectric-continuum approximation, the potential $V(\mathbf{r})$ of polar optical phonons satisfies the Maxwell equation, which can be written in the coordinates $\mathbf{r}=(x,\ y,\ z)$ as

$$-\nabla(\hat{\varepsilon}(\omega,\mathbf{r})\nabla V(\mathbf{r}))=0 \tag{5}$$

with the dielectric tensor $\hat{\varepsilon}(\omega,\mathbf{r})$ defined as

$$\hat{\varepsilon}(\omega,\mathbf{r})=\begin{pmatrix}\varepsilon_\perp(\omega,\mathbf{r}) & 0 & 0\\ 0 & \varepsilon_\perp(\omega,\mathbf{r}) & 0\\ 0 & 0 & \frac{a^2}{c^2}\varepsilon_z(\omega,\mathbf{r})\end{pmatrix}. \tag{6}$$

Note that the term a^2/c^2 appears in equation (6) due to the coordinate transformation (4). The dielectric tensor (6) is constant in both media,

$$\hat{\varepsilon}(\omega, \mathbf{r}) = \begin{cases} \hat{\varepsilon}_1(\omega), & r \leqslant a; \\ \hat{\varepsilon}_2(\omega), & r > a, \end{cases} \tag{7}$$

therefore it is convenient to split equation (5) into separate equations for each medium,

$$-\nabla(\hat{\varepsilon}_k(\omega)\nabla V_k(\mathbf{r})) = 0; \qquad k = 1, 2 \tag{8}$$

and apply the corresponding boundary conditions:

$$V_1(a, \theta, \phi) = V_2(a, \theta, \phi); \tag{9}$$

$$D_1(a, \theta, \phi) = D_2(a, \theta, \phi), \tag{10}$$

where the projections of the displacement vector $\mathbf{D}$ on the outer normal $\mathbf{n}$ at the quantum dot surface can be written as

$$D_k(a, \theta, \phi) = (\mathbf{n}(\mathbf{r})\hat{\varepsilon}_k(\omega)\nabla V_k(\mathbf{r}))\big|_{r=a}; \qquad k = 1, 2. \tag{11}$$

The phonon potential $V_1(\mathbf{r})$ that satisfies equation (8) and is finite everywhere inside the quantum dot can be found analytically in spheroidal coordinates (ξ_1, η_1, ϕ):

$$V_1(\mathbf{r}) = \frac{P_l^m(\xi_1)}{P_l^m(\xi_1^{(0)})} P_l^m(\eta_1) \mathrm{e}^{\mathrm{i}m\phi}. \tag{12}$$

Analogously, the phonon potential $V_2(\mathbf{r})$ that satisfies equation (8) and vanishes far away from the quantum dot can be found analytically in spheroidal coordinates (ξ_2, η_2, ϕ):

$$V_2(\mathbf{r}) = \frac{Q_l^m(\xi_2)}{Q_l^m(\xi_2^{(0)})} P_l^m(\eta_2) \mathrm{e}^{\mathrm{i}m\phi}. \tag{13}$$

In equations (12) and (13), P_l^m and Q_l^m are associated Legendre functions of the first and second kinds, respectively; the integers l ($l \geqslant 0$) and m ($|m| \leqslant l$) are quantum numbers of the phonon mode. The spheroidal coordinates (ξ_k, η_k) are related to the spherical coordinates (r, θ) as

$$\begin{aligned} r\sin\theta &= a\sqrt{\left(\frac{1}{g_k(\omega)} - 1\right)(\xi_k^2 - 1)}\sqrt{1 - \eta_k^2}, \\ r\cos\theta &= a\sqrt{1 - g_k(\omega)}\xi_k\eta_k, \end{aligned} \tag{14}$$

where $k = 1, 2$ and

$$g_k(\omega) = \frac{a^2}{c^2}\frac{\varepsilon_z^{(k)}(\omega)}{\varepsilon_\perp^{(k)}(\omega)}. \tag{15}$$

The range of the spheroidal coordinate η_k is $-1 \leqslant \eta_k \leqslant 1$. Depending on the value of the function (15), the spheroidal coordinate ξ_k can have the following range:

$$\begin{aligned} &0 < \xi_k < 1 && \text{if } g_k(\omega) < 0; \\ &\xi_k > 1 && \text{if } 0 < g_k(\omega) < 1; \\ &\mathrm{i}\xi_k > 0 && \text{if } g_k(\omega) > 1. \end{aligned} \tag{16}$$

According to equation (14), the quantum dot surface $r = a$ is defined in the spheroidal coordinates as

$$\begin{aligned} \xi_k &= \xi_k^{(0)} \equiv 1/\sqrt{1 - g_k(\omega)}, \\ \eta_k &= \cos\theta. \end{aligned} \tag{17}$$

Therefore, the part of the phonon potential $V_1(\mathbf{r})$ defined by equation (12) and the part of the phonon potential $V_2(\mathbf{r})$ defined by equation (13) coincide at the quantum dot surface. Thus, the first boundary condition, given by equation (9), is satisfied.

Now, let us find the normal component of the displacement vector $\mathbf{D}$ at the quantum dot surface. According to equation (11),

$$D_k(a,\theta,\phi)=\varepsilon_{\perp}^{(k)}(\omega)\left[(g_k(\omega)\cos^2\theta+\sin^2\theta)\left.\frac{\partial V_k}{\partial r}\right|_{r=a}+\frac{1-g_k(\omega)}{a}\sin\theta\cos\theta\left.\frac{\partial V_k}{\partial\theta}\right|_{r=a}\right]. \tag{18}$$

Using relation (14) between the coordinates (ξ_k,η_k) and (r,θ), we can calculate each of the two partial derivatives from equation (18):

$$\left.\frac{\partial V_k}{\partial r}\right|_{r=a}=\frac{1}{a(g_k(\omega)\cos^2\theta+\sin^2\theta)}\times\left[\frac{g_k(\omega)}{\sqrt{1-g_k(\omega)}}\left.\frac{\partial V_k}{\partial\xi_k}\right|_{\substack{\xi_k=\xi_k^{(0)}\\ \eta_k=\cos\theta}}+\cos\theta\sin^2\theta(1-g_k(\omega))\left.\frac{\partial V_k}{\partial\eta_k}\right|_{\substack{\xi_k=\xi_k^{(0)}\\ \eta_k=\cos\theta}}\right], \tag{19}$$

$$\left.\frac{\partial V_k}{\partial\theta}\right|_{r=a}=-\sin\theta\left.\frac{\partial V_k}{\partial\eta_k}\right|_{\substack{\xi_k=\xi_k^{(0)}\\ \eta_k=\cos\theta}}. \tag{20}$$

Substituting equations (19) and (20) into (18), one obtains a simple formula:

$$D_k(a,\theta,\phi)=\frac{\varepsilon_{\perp}^{(k)}(\omega)g_k(\omega)}{a\sqrt{1-g_k(\omega)}}\left.\frac{\partial V_k}{\partial\xi_k}\right|_{\substack{\xi_k=\xi_k^{(0)}\\ \eta_k=\cos\theta}}. \tag{21}$$

Finally, using the explicit form of the phonon potentials (12) and (13) as well as equations (15) and (17), one can rewrite equation (21) as

$$D_1(a,\theta,\phi)=\frac{a}{c^2}\frac{\varepsilon_z^{(1)}(\omega)}{\sqrt{1-g_1(\omega)}}\left.\frac{\mathrm{d}\ln P_l^m(\xi_1)}{\mathrm{d}\xi_1}\right|_{\xi_1=\xi_1^{(0)}}P_l^m(\cos\theta)\mathrm{e}^{\mathrm{i}m\phi}; \tag{22}$$

$$D_2(a,\theta,\phi)=\frac{a}{c^2}\frac{\varepsilon_z^{(2)}(\omega)}{\sqrt{1-g_2(\omega)}}\left.\frac{\mathrm{d}\ln Q_l^m(\xi_2)}{\mathrm{d}\xi_2}\right|_{\xi_2=\xi_2^{(0)}}P_l^m(\cos\theta)\mathrm{e}^{\mathrm{i}m\phi}. \tag{23}$$

Substituting equations (22) and (23) into the second boundary condition (10), one can see that it is satisfied only when the following equality is true:

$$\varepsilon_z^{(1)}(\omega)\left(\xi\frac{\mathrm{d}\ln P_l^m(\xi)}{\mathrm{d}\xi}\right)\Bigg|_{\xi=1/\sqrt{1-g_1(\omega)}}=\varepsilon_z^{(2)}(\omega)\left(\xi\frac{\mathrm{d}\ln Q_l^m(\xi)}{\mathrm{d}\xi}\right)\Bigg|_{\xi=1/\sqrt{1-g_2(\omega)}}. \tag{24}$$

Thus, we have obtained the equation that defines the spectrum of polar optical phonons in a wurtzite spheroidal quantum dot embedded in a wurtzite crystal. Note that equation (24) can be also obtained using a completely different technique developed by us for wurtzite nanocrystals of arbitrary shape [8]. It should be pointed out that for a spheroidal quantum dot with zincblende crystal structure $\varepsilon_{\perp}^{(k)}(\omega)=\varepsilon_z^{(k)}(\omega)\equiv\varepsilon^{(k)}(\omega)$ and equation (24) reduces to the one obtained in [2, 3]. The fact that the spectrum of polar optical phonons does not depend on the absolute size of a quantum dot [1, 2] is also seen from equation (24).

The case of a freestanding quantum dot is no less important for practical applications. In this case the dielectric tensor of the exterior medium is a constant $\varepsilon_{\mathrm{D}}\equiv\varepsilon_z^{(2)}(\omega)=\varepsilon_{\perp}^{(2)}(\omega)$. Therefore, using the explicit form of associated Legendre polynomials P_l^m and omitting the

upper index '(1)' in the components of the dielectric tensor of the quantum dot, we can represent equation (24) in the following convenient form:

$$\sum_{n=0}^{\left\lfloor \frac{l-|m|}{2} \right\rfloor} \left[\frac{c^2}{a^2} \frac{\varepsilon_\perp(\omega)}{\varepsilon_{\rm D}} |m| + \frac{\varepsilon_z(\omega)}{\varepsilon_{\rm D}} (l - |m| - 2n) - f_l^{|m|}\left(\frac{a}{c}\right) \right] \times \binom{l-|m|}{2n} \frac{(2n-1)!!(2l-2n-1)!!}{(2l-1)!!} \left[\frac{a^2}{c^2} \frac{\varepsilon_z(\omega)}{\varepsilon_\perp(\omega)} - 1 \right]^n = 0, \tag{25}$$

where

$$f_l^m(\alpha) = \xi \left. \frac{{\rm d} \ln Q_l^m(\xi)}{{\rm d}\xi} \right|_{\xi = 1/\sqrt{1-\alpha^2}}. \tag{26}$$

It can be shown that the function $f_l^m(\alpha)$ increases monotonically from $-\infty$ to 0 when α increases from 0 to ∞. As seen from equation (25), there are no phonon modes with $l = 0$ and all phonon frequencies with $m \neq 0$ are twice degenerate with respect to the sign of m. For a spherical ($\alpha = 1$) freestanding quantum dot one has to take the limit $\xi \to \infty$ in equation (26), which results in $f_l^m(1) = -(l+1)$. Thus, in the case of a zincblende spherical quantum dot ($\varepsilon_\perp(\omega) = \varepsilon_z(\omega) \equiv \varepsilon(\omega)$; $a = c$), equation (25) gives the well known equation $\varepsilon(\omega)/\varepsilon_{\rm D} = -1 - 1/l$ derived in [1].

3. Freestanding ZnO quantum dots

In this section we consider freestanding spheroidal ZnO quantum dots and examine the phonon modes with quantum numbers $l = 1, 2, 3, 4$ and $m = 0, 1$. The components of the dielectric tensor of wurtzite ZnO are given by equation (1). The exterior medium is considered to be air with $\varepsilon_{\rm D} = 1$. Figure 2 shows the spectrum of polar optical phonons with $m = 0$ and figure 3 shows the spectrum of polar optical phonons with $m = 1$. The frequencies with even l are plotted with solid curves while the frequencies with odd l are plotted with dashed curves. The frequencies in figures 2 and 3 are found as solutions of equation (25) and are plotted as a function of the ratio of the spheroidal semi-axes a and c. Thus, in the leftmost part of the plots we have the phonon spectrum for a spheroid degenerated into a vertical line segment; farther to the right we have the spectrum for prolate spheroids; in the central part of the plots we have the phonon spectrum for a sphere; farther on we have the spectrum for oblate spheroids; and in the rightmost part of the plots we have the phonon spectrum for a spheroid degenerated into a horizontal flat disc.

The calculated spectrum of phonons in the freestanding ZnO quantum dots can be divided into three regions: confined TO phonons ($\omega_{z,{\rm TO}} < \omega < \omega_{\perp,{\rm TO}}$), interface phonons ($\omega_{\perp,{\rm TO}} < \omega < \omega_{z,{\rm LO}}$), and confined LO phonons ($\omega_{z,{\rm LO}} < \omega < \omega_{\perp,{\rm LO}}$). The above division into confined and interface phonons is based on the sign of the function $g(\omega)$ (see equation (15)). We call the phonons with eigenfrequency ω interface phonons if $g(\omega) > 0$ and confined phonons if $g(\omega) < 0$. To justify the classification of phonon modes as interface and confined ones based on the sign of the function $g_1(\omega)$, let us consider the phonon potential (12) inside the quantum dot. If $g_1(\omega) < 0$ then, according to equation (16), $0 < \xi_1 < 1$; therefore, $P_l^m(\xi_1)$ is an oscillatory function of ξ_1 and the phonon potential (12) is mainly confined inside the quantum dot. If, on the contrary, $g_1(\omega) > 0$, then, according to equation (16), $\xi_1 > 1$ or ${\rm i}\xi_1 > 0$; therefore $P_l^m(\xi_1)$ increases monotonically with ξ_1 as ξ_1^l, reaching the maximum at the quantum dot surface together with the phonon potential (12). Note that the vertical frequency scale in figures 2 and 3 is different for confined TO, interface, and confined LO phonons. The true scale is shown in figure 1.

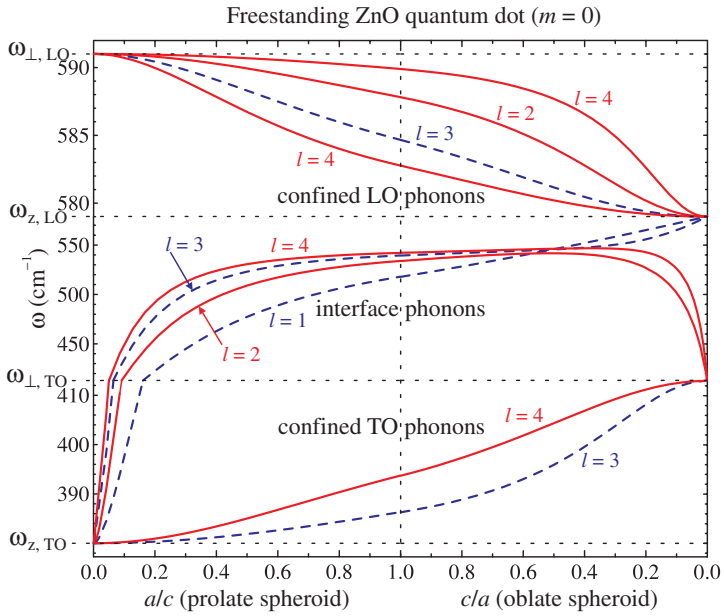

Figure 2. Frequencies of polar optical phonons with $l = 1, 2, 3, 4$ and $m = 0$ for a freestanding spheroidal ZnO quantum dot as a function of the ratio of spheroidal semi-axes. Solid curves correspond to phonons with even l and dashed curves correspond to phonons with odd l. The frequency scale is different for confined TO, interface, and confined LO phonons.

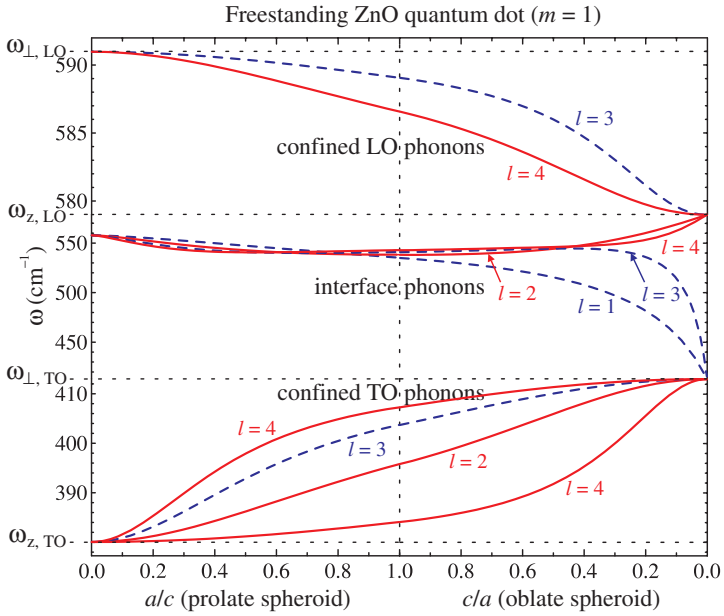

Figure 3. The same as figure 2 but for polar optical phonons with $m = 1$.

Analysing equation (25), one can find that for each pair (l, m) there is one interface optical phonon and $l - |m|$ confined optical phonons for $m \neq 0$ ($l - 1$ for $m = 0$). Therefore, we

can see four interface phonons and six confined phonons for both $m = 0$ and 1 in figures 2 and 3. However, one can see that there are four confined LO phonons with $m = 0$ and only two confined LO phonons with $m = 1$. In contrast, there are only two confined TO phonons with $m = 0$ and four confined TO phonons with $m = 1$ in figures 2 and 3.

When the shape of the spheroidal quantum dot changes from the vertical line segment to the horizontal flat disc, the frequencies of all confined LO phonons decrease from $\omega_{\perp,\mathrm{LO}}$ to $\omega_{z,\mathrm{LO}}$. At the same time the frequencies of all confined TO phonons increase from $\omega_{z,\mathrm{TO}}$ to $\omega_{\perp,\mathrm{TO}}$. It is also seen from figures 2 and 3 that for very small ratios a/c, which is the case of so-called quantum rods, the interface phonons with $m = 0$ become confined TO phonons, while the frequencies of all interface phonons with $m = 1$ degenerate into a single frequency. When the shape of the spheroidal quantum dot changes from the vertical line segment to the horizontal flat disc, the frequencies of interface phonons with odd l and $m = 0$ increase from $\omega_{z,\mathrm{TO}}$ to $\omega_{z,\mathrm{LO}}$, while the frequencies of interface phonons with even l and $m = 0$ increase for prolate spheroids starting from $\omega_{z,\mathrm{TO}}$, as for the phonons with odd l, but they farther decrease up to $\omega_{\perp,\mathrm{TO}}$ for oblate spheroids. In contrast, when the shape of the spheroidal quantum dot changes from the vertical line segment to the horizontal flat disc, the frequencies of interface phonons with odd l and $m = 1$ decrease from a single interface frequency to $\omega_{\perp,\mathrm{TO}}$, while the frequencies of interface phonons with even l and $m = 1$ decrease for prolate spheroids starting from a single frequency, as for the phonons with odd l, but they increase farther up to $\omega_{z,\mathrm{LO}}$ for oblate spheroids.

In the rest of this section we study phonon potentials corresponding to the polar optical phonon modes with $l = 1, 2, 3, 4$ and $m = 0$. In figure 4 we present the phonon potentials for a spherical freestanding ZnO quantum dot. The phonon potentials for quantum dots with arbitrary spheroidal shapes can be found analogously using equations (12) and (13) and the coordinate transformation (4). As seen from figure 4, the confined LO phonons are, indeed, confined inside the quantum dot. However, unlike confined phonons in zincblende quantum dots, confined phonons in wurtzite quantum dots slightly penetrate into the exterior medium. The potential of interface phonon modes is, indeed, localized near the surface of the wurtzite quantum dot. While there are no confined TO phonons in zincblende quantum dots, they appear in wurtzite quantum dots. It is seen from figure 4 that confined TO phonons are, indeed, localized mainly inside the quantum dot. However, they penetrate into the exterior medium much more strongly than confined LO phonons.

Using the theory of excitonic states in wurtzite quantum dots [13, 14], it can be shown that the dominant component of the wavefunction of the exciton ground state in spheroidal ZnO quantum dots is symmetric with respect to the rotations around the z-axis or reflection in the xy-plane. Therefore, the selection rules for the polar optical phonon modes observed in the resonant Raman spectra of ZnO quantum dots are $m = 0$ and $l = 2, 4, 6, \ldots$. The phonon modes with higher symmetry (smaller quantum number l) are more likely to be observed in the Raman spectra. It is seen from figure 4, that the confined LO phonon mode with $l = 2$, $m = 0$ and the confined TO mode with $l = 4$, $m = 0$ are the confined modes with the highest symmetry among the confined LO and TO phonon modes, correspondingly. Therefore, they should give the main contribution to the resonant Raman spectrum of spheroidal ZnO quantum dots.

In fact, the above conclusion has an experimental confirmation. In the resonant Raman spectrum of spherical ZnO quantum dots with diameter 8.5 nm from [15], the main Raman peak in the region of LO phonons has the frequency 588 cm^{-1} and the main Raman peak in the region of TO phonons has the frequency 393 cm^{-1}. In accordance with figure 2, our calculations give the frequency 587.8 cm^{-1} of the confined LO phonon mode with $l = 2$, $m = 0$ and the frequency 393.7 cm^{-1} of the confined TO phonon mode with $l = 4$, $m = 0$.

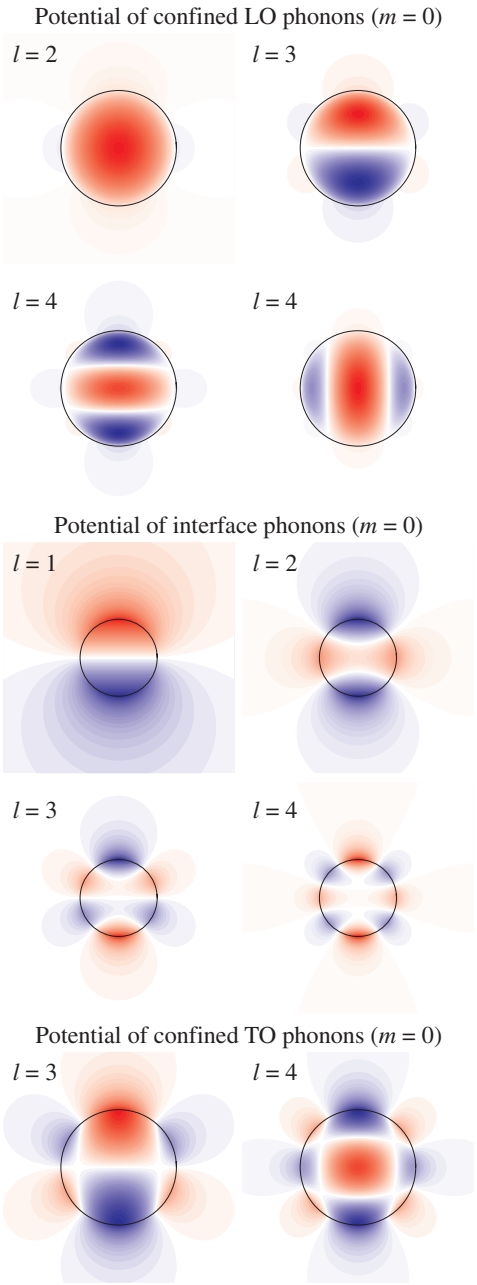

Figure 4. Cross-sections of phonon potentials corresponding to polar optical phonon modes with $l = 1, 2, 3, 4$ and $m = 0$ for the freestanding spherical ZnO quantum dot. The Z-axis is directed vertically. In the colour version blue and red colours denote negative and positive values of phonon potentials, correspondingly. The black circle represents the quantum dot surface.

This excellent agreement of the experimental and calculated frequencies allows one to predict the main peaks in the LO and TO regions of a Raman spectra of spheroidal ZnO quantum dots using the corresponding curves from figure 2.

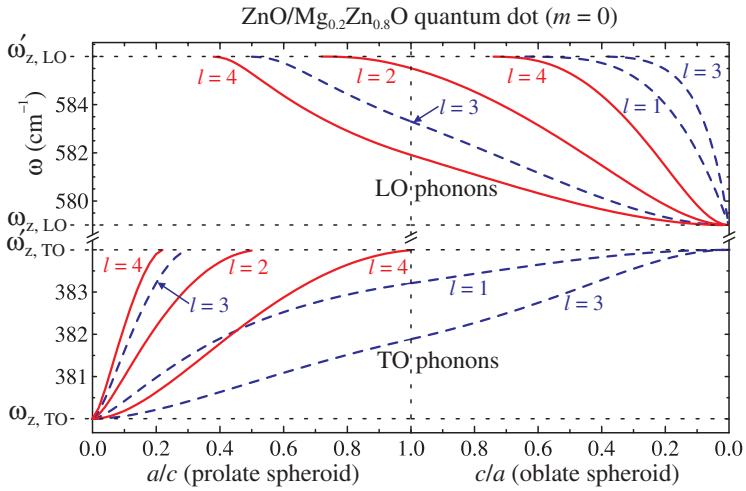

Figure 5. Frequencies of polar optical phonons with $l = 1, 2, 3, 4$ and $m = 0$ for a spheroidal ZnO/$Mg_{0.2}Zn_{0.8}O$ quantum dot as a function of the ratio of spheroidal semi-axes. Solid curves correspond to phonons with even l and dashed curves correspond to phonons with odd l. The frequency scale is different for TO and LO phonons. Frequencies $\omega_{z,\mathrm{TO}}$ and $\omega_{z,\mathrm{LO}}$ correspond to ZnO and frequencies $\omega'_{z,\mathrm{TO}}$ and $\omega'_{z,\mathrm{LO}}$ correspond to $Mg_{0.2}Zn_{0.8}O$.

4. ZnO/MgZnO quantum dots

In this section we consider spheroidal ZnO quantum dots embedded into a $Mg_{0.2}Zn_{0.8}O$ crystal. The components of the dielectric tensors of wurtzite ZnO and $Mg_{0.2}Zn_{0.8}O$ are given by equations (1) and (2), correspondingly. The relative position of optical phonon bands of wurtzite ZnO and $Mg_{0.2}Zn_{0.8}O$ is shown in figure 1. It is seen from equation (15) that $g_1(\omega) < 0$ inside the shaded region corresponding to ZnO in figure 1 and $g_2(\omega) < 0$ inside the shaded region corresponding to $Mg_{0.2}Zn_{0.8}O$. As it has been shown in section 3, the frequency region where $g_1(\omega) < 0$ corresponds to confined phonons in a freestanding spheroidal ZnO quantum dot. However, there can be no confined phonons in the host $Mg_{0.2}Zn_{0.8}O$ crystal. Indeed, there are no physical solutions of equation (24) when $g_2(\omega) < 0$. The solutions of equation (24) are nonphysical in this case, because the spheroidal coordinates (ξ_2, η_2) defined by equation (14) cannot cover the entire space outside the quantum dot. If we allow the spheroidal coordinates (ξ_2, η_2) to be complex, then the phonon potential outside the quantum dot becomes complex and diverges logarithmically when $\xi_2 = 1$; the latter is clearly nonphysical. It can also be shown that equation (24) does not have any solutions when $g_1(\omega) > 0$ and $g_2(\omega) > 0$. Therefore, the only case when equation (24) allows for physical solutions is $g_1(\omega) < 0$ and $g_2(\omega) > 0$. The frequency regions that satisfy the latter condition are cross-hatched in figure 1. There are two such regions: $\omega^{(1)}_{z,\mathrm{TO}} < \omega < \omega^{(2)}_{z,\mathrm{TO}}$ and $\omega^{(1)}_{z,\mathrm{LO}} < \omega < \omega^{(2)}_{z,\mathrm{LO}}$, which are further called the regions of TO and LO phonons, respectively.

Let us now examine the LO and TO phonon modes with quantum numbers $l = 1, 2, 3, 4$ and $m = 0, 1$. Figure 5 shows the spectrum of polar optical phonons with $m = 0$ and figure 6 shows the spectrum of polar optical phonons with $m = 1$. The frequencies with even l are plotted with solid curves while the frequencies with odd l are plotted with dashed curves. The frequencies in figures 5 and 6 are found as solutions of equation (24) and are plotted as a function of the ratio of the spheroidal semi-axes a and c, similarly to figures 2 and 3 for the freestanding spheroidal ZnO quantum dot. Note that the vertical frequency scale in figures 5 and 6 is different for TO phonons and LO phonons. The true scale is shown in figure 1.

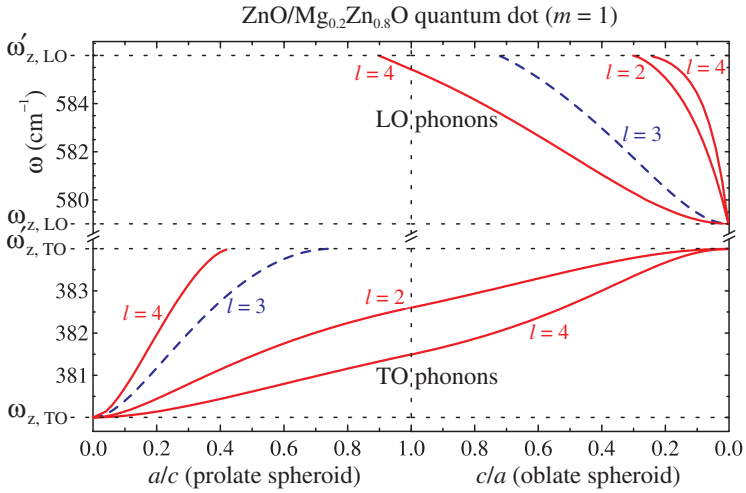

Figure 6. The same as figure 5 but for polar optical phonons with $m = 1$.

Comparing figure 5 with 2 and figure 6 with 3 we can see the similarities and distinctions in the phonon spectra of the ZnO quantum dot embedded into the $Mg_{0.2}Zn_{0.8}O$ crystal and that of the freestanding ZnO quantum dot. For a small ratio a/c we have the same number of TO phonon modes with the frequencies originating from $\omega^{(1)}_{z,\mathrm{TO}}$ for the embedded and freestanding ZnO quantum dots. With the increase of the ratio a/c the frequencies of TO phonons increase for both embedded and freestanding ZnO quantum dots, but the number of TO phonon modes gradually decreases in the embedded ZnO quantum dot. When $a/c \to \infty$ only two phonon modes with odd l are left for $m = 0$ and two phonon modes with even l are left for $m = 1$. The frequencies of these phonon modes increase up to $\omega^{(2)}_{z,\mathrm{TO}}$ when $a/c \to \infty$. However, for this small ratio c/a we have the same number of LO phonon modes with the frequencies originating from $\omega^{(1)}_{z,\mathrm{LO}}$ for the embedded and freestanding ZnO quantum dots. With the increase of the ratio c/a the frequencies of all LO phonons increase for the embedded ZnO quantum dot and the number of such phonons gradually decreases. When $c/a \to \infty$ there are no phonons left for the embedded ZnO quantum dot. At the same time for the freestanding ZnO quantum dot, with the increase of the ratio c/a, the frequencies of two LO phonons with odd l and $m = 0$ and two LO phonons with even l and $m = 1$ decrease and go into the region of interface phonons.

It is seen from the previous paragraph that for the ZnO quantum dot with a small ratio c/a embedded into the $Mg_{0.2}Zn_{0.8}O$ crystal the two LO and two TO phonon modes with odd l and $m = 0$ and with even l and $m = 1$ may correspond to interface phonons. To check this hypothesis, we further study phonon potentials corresponding to the polar optical phonon modes with $l = 1, 2, 3, 4$ and $m = 0$. In figure 7 we present the phonon potentials for the spheroidal ZnO quantum dot with the ratio $c/a = 1/4$ embedded into the $Mg_{0.2}Zn_{0.8}O$ crystal. The considered ratio $c/a = 1/4$ of the spheroidal semi-axes is a reasonable value for epitaxial ZnO/ $Mg_{0.2}Zn_{0.8}O$ quantum dots. It is seen in figure 7 that the LO phonon with $l = 1$, one of the LO phonons with $l = 3$, and all two TO phonons are, indeed, interface phonons, since they achieve their maximal and minimal values at the surface of the ZnO quantum dot. It is interesting that the potential of interface TO phonons is strongly extended along the z-axis, while the potential of interface LO phonons is extended in the xy-plane. All other LO phonons in figure 7 are confined. The most symmetrical phonon mode is, again, the one with $l = 2$ and $m = 0$. Therefore, it should give the main contribution to the Raman spectrum

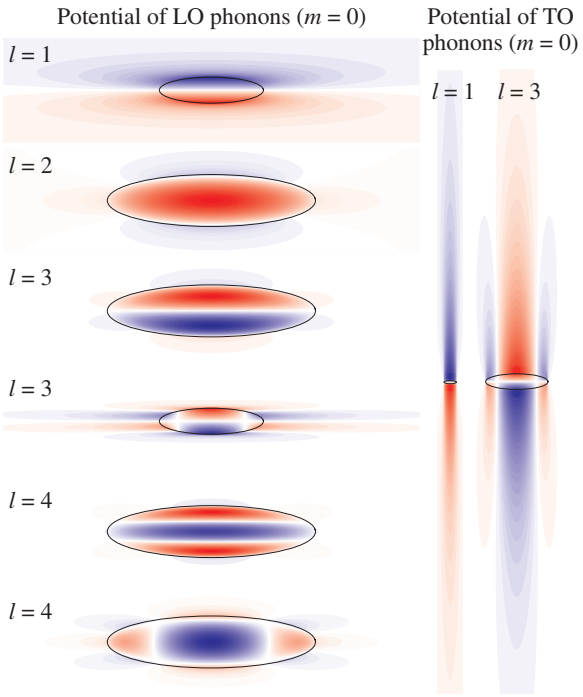

Figure 7. Cross-sections of phonon potentials corresponding to polar optical phonon modes with $l = 1, 2, 3, 4$ and $m = 0$ for the oblate spheroidal ZnO/$Mg_{0.2}Zn_{0.8}O$ quantum dot with aspect ratio $1/4$. The Z-axis is directed vertically. In the colour version blue and red colours denote negative and positive values of phonon potentials, correspondingly. The black ellipse represents the quantum dot surface.

of oblate spheroidal ZnO quantum dots embedded into the $Mg_{0.2}Zn_{0.8}O$ crystal. Unlike the case for freestanding ZnO quantum dots, no pronounced TO phonon peaks are expected for the embedded ZnO quantum dots.

5. Conclusions

In conclusion, we have derived analytically interface and confined polar optical phonon modes for spheroidal quantum dots with wurtzite crystal structure. The developed theory has been applied to study phonon frequencies and potentials as a function of the ratio of spheroidal semi-axes for freestanding spheroidal ZnO quantum dots and spheroidal ZnO quantum dots embedded into the $Mg_{0.2}Zn_{0.8}O$ crystal. Similarly to the case of spheroidal quantum dots with zincblende crystal structure, a discrete spectrum of frequencies has been obtained for *interface* polar optical phonons in wurtzite spheroidal quantum dots. At the same time, the discrete spectrum of frequencies has been also found for *confined* polar optical phonons in wurtzite quantum dots, while the confined polar optical phonons in zincblende quantum dots have a single frequency (LO). The positions of polar optical-phonon lines observed in the resonant Raman spectra of spherical wurtzite ZnO quantum dots have been explained quantitatively. The obtained theoretical results allow one to explain and accurately predict phonon peaks in the Raman spectra not only for wurtzite ZnO nanocrystals, nanorods, and epitaxial ZnO/$Mg_{0.2}Zn_{0.8}O$ quantum dots, but also for any wurtzite spheroidal quantum dot, either freestanding or embedded into another crystal.

Acknowledgments

This work was supported in part by the Microelectronics Advanced Research Corporation (MARCO) and its Focus Center on Functional Engineered Nano Architectonics (FENA), NSF-NATO 2003 award to VAF, ONR Young Investigator Award to AAB, and DMEA/DARPA CNID programme A01809-23103-44.

References

[1] Englman R and Ruppin R 1966 *Phys. Rev. Lett.* **16** 898
[2] Knipp P A and Reinecke T L 1992 *Phys. Rev.* B **46** 10310
[3] Comas F, Trallero-Giner G, Studart N and Marques G E 2002 *Phys. Rev.* B **65** 073303
Comas F, Trallero-Giner G, Studart N and Marques G E 2002 *J. Phys.: Condens. Matter* **14** 6469
[4] Klimin S N, Pokatilov E P and Fomin V M 1994 *Phys. Status Solidi* b **184** 373
[5] Fonoberov V A, Pokatilov E P, Fomin V M and Devreese J T 2004 *Phys. Rev. Lett.* **92** 127402
[6] Pokatilov E P, Klimin S N, Fomin V M, Devreese J T and Wise F W 2002 *Phys. Rev.* B **65** 075316
[7] Romanov D, Mitin V and Stroscio M 2002 *Physica* E **12** 491
Romanov D A, Mitin V V and Stroscio M A 2002 *Phys. Rev.* B **66** 115321
[8] Fonoberov V A and Balandin A A 2004 *Phys. Rev.* B **70** 233205
[9] Stroscio M A and Dutta M 2001 *Phonons in Nanostructures* (Cambridge: Cambridge University Press)
[10] Chen C, Dutta M and Stroscio M A 2004 *J. Appl. Phys.* **95** 2540
Chen C, Dutta M and Stroscio M A 2004 *Phys. Rev.* B **70** 075316
Chen C, Dutta M and Stroscio M A 2004 *J. Appl. Phys.* **96** 2049
[11] Arguello C A, Rousseau D L and Porto S P S 1969 *Phys. Rev.* **181** 1351
[12] Bundesmann C, Schubert M, Spemann D, Butz T, Lorenz M, Kaidashev E M, Grundmann M, Ashkenov N, Neumann H and Wagner G 2002 *Appl. Phys. Lett.* **81** 2376
[13] Fonoberov V A and Balandin A A 2004 *Phys. Rev.* B **70** 195410
Fonoberov V A and Balandin A A 2004 *Appl. Phys. Lett.* **85** 5971
[14] Fonoberov V A and Balandin A A 2003 *J. Nanosci. Nanotechnol.* **3** 253
Fonoberov V A and Balandin A A 2003 *J. Appl. Phys.* **94** 7178
Fonoberov V A and Balandin A A 2004 *J. Vac. Sci. Technol.* B **22** 2190
[15] Rajalakshmi M, Arora A K, Bendre B S and Mahamuni S 2000 *J. Appl. Phys.* **87** 2445